Recordings from Single Neocortical Nerve Terminals Reveal a Nonselective Cation Channel Activated by Decreases in Extracellular Calcium

Stephen M. Smith,[1,2,4,5] Jeremy B. Bergsman,[1,3,5,6]
Nobutoshi C. Harata,[1] Richard H. Scheller,[1,2,7]
and Richard W. Tsien[1,*]
[1]Department of Molecular and Cellular Physiology
[2]Howard Hughes Medical Institute
[3]Neurosciences Program
Beckman Center
Stanford University School of Medicine
Stanford, California 94305
[4]Division of Molecular Medicine
Division of Pulmonary & Critical Care Medicine
Oregon Health & Science University
Portland, Oregon 97201

Summary

Synaptic activity causes reductions in cleft $[Ca^{2+}]$ that may impact subsequent synaptic efficacy. Using modified patch-clamp techniques to record from single neocortical nerve terminals, we report that physiologically relevant reductions of extracellular $[Ca^{2+}]$ ($[Ca^{2+}]_o$) activate voltage-dependent outward currents. These outward currents are carried by a novel nonselective cation (NSC) channel that is indirectly inhibited by various extracellular agents (rank order potency, Gd^{3+} > spermidine > Ca^{2+} > Mg^{2+}, typical for $[Ca^{2+}]_o$ receptors). The identification of a Ca^{2+} sensor-NSC channel pathway establishes the existence of a mechanism by which presynaptic terminals can detect and respond to reductions in cleft $[Ca^{2+}]$. Activation of NSC channels by falls in $[Ca^{2+}]_o$ would be expected during periods of high activity in the neocortex and may modulate the excitability of the presynaptic terminal.

Introduction

Neurotransmission at central excitatory synapses is associated with entry of Ca^{2+} into both pre- and postsynaptic neurons, leading to significant reductions in the external Ca^{2+} concentration. Ion-selective electrode measurements in the intact brain have shown that bulk $[Ca^{2+}]_o$ decreases to 0.8 mM following direct cortical stimulation (Nicholson et al., 1978) and to 0.1 mM after pathological insults (Nilsson et al., 1996). One factor that helps prolong falls in $[Ca^{2+}]_o$ is the slowing of diffusion in the extracellular space, which may be as great as 5-fold compared with free solution, due to geometrical tortuosity and Ca^{2+} binding to molecules along its diffusion path (Kullmann et al., 1999).

$[Ca^{2+}]_o$ is particularly likely to undergo activity-dependent depletion in the synaptic cleft, a small, restricted volume with a high density of Ca^{2+}-depleting mechanisms on both its pre- and postsynaptic borders. Proposals that Ca^{2+} influx during neurotransmission will significantly reduce cleft $[Ca^{2+}]$ date back more than ten years (Egelman and Montague, 1999; Smith, 1992; Vassilev et al., 1997). Although direct measurements of cleft $[Ca^{2+}]$ have been prevented by lack of access to the synaptic cleft, inferences have been made at unusually large synapses by comparing Ca^{2+} channel currents before and after presynaptic depolarization (Borst and Sakmann, 1999a; Rabl and Thoreson, 2002; Stanley, 2000). With basal Ca^{2+} or Ba^{2+} set at 1.8–5 mM, depolarization of the pre- or postsynaptic element reduced the cleft $[Ca^{2+}]$ or $[Ba^{2+}]$ by 30%–60%. An even greater fractional change in cleft $[Ca^{2+}]$ would be expected with basal $[Ca^{2+}]_o$ at physiological levels ($\sim$1.1 mM). The efficacy of the nerve terminal as a Ca^{2+} sink is emphasized by studies in the neurohypophysis, a collection of nerve endings, where increases of intracellular $[Ca^{2+}]$ ($[Ca^{2+}]_i$) during the release of vasopressin were mirrored by falls in $[Ca^{2+}]_o$ (Shibuki, 1990). Additional experiments in hippocampal slices showed that $[Ca^{2+}]_o$ can also be reduced by postsynaptic mechanisms (Rusakov and Fine, 2003). If movement of Ca^{2+} into pre- and postsynaptic elements drives a general Ca^{2+} depletion in bulk, the measured declines in global $[Ca^{2+}]_o$ in brain tissue would be underestimates of the true degree of depletion in the synaptic cleft.

In contrast to the wealth of information about intracellular Ca^{2+} signaling, much less is known about the impact of changes in $[Ca^{2+}]_o$. Although it was proposed that a decrease in cleft $[Ca^{2+}]$ may provide an important signal to the nerve terminal (Smith, 1992; Vassilev et al., 1997), direct and meaningful sensing of $[Ca^{2+}]_o$ by presynaptic elements has not yet been found. What has been reported are numerous instances of $[Ca^{2+}]_o$ sensing and modulation of ion channels in neuron cell bodies and axons (Armstrong and Cota, 1999; Formenti et al., 2001; Hablitz et al., 1986; Immke and McCleskey, 2001; Xiong et al., 1997), some perhaps due to changes in surface charge (Frankenhaeuser and Hodgkin, 1957).

Mindful that the most significant drops of $[Ca^{2+}]_o$ should occur in the synaptic cleft, we investigated the effect of reductions in $[Ca^{2+}]_o$ on ion channel activity in pinched-off cortical nerve terminals (synaptosomes). We succeeded in making direct patch clamp recordings from synaptosomes and used this approach to explore how the presynaptic terminal responds to lowering of $[Ca^{2+}]_o$.

Results

Functional and Structural Integrity of Synaptosomes

We plated synaptosomes onto glass coverslips to facilitate recordings from single nerve terminals. They spontaneously formed clusters of varying size (Figure 1A, left). As synaptosomes in suspension release neurotransmitter in a voltage- and Ca^{2+}-dependent manner

*Correspondence: rwtsien@stanford.edu
[5]These authors contributed equally to this work.
[6]Present address: Departments of Cell Biology and Neurobiology, Yale University School of Medicine, P.O. Box 208001, New Haven, Connecticut 06520.
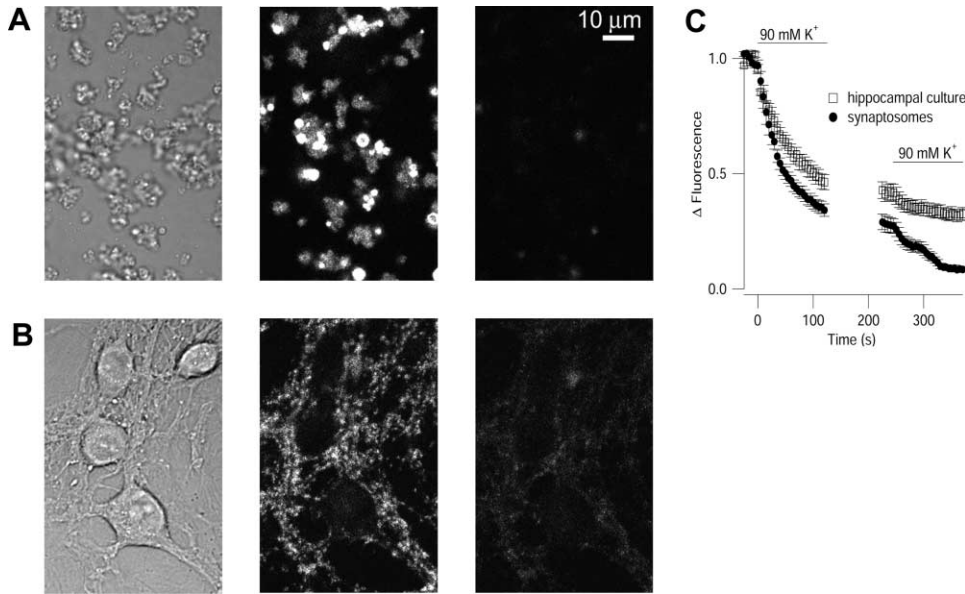[7]Present address: Genentech, Inc., 1 DNA Way, S. San Francisco, California 94080.

Figure 1. Characterization of Plated Synaptosomes by Light Microscopy

(A and B) Plated synaptosomes (A) and hippocampal neurons (B) in DIC images (left), FM 1-43 fluorescence after staining (middle), and FM 1-43 fluorescence after two bouts of destaining with 90 mM K^+ (right).
(C) Similar kinetics of destaining of synaptosomes (n = 21) and hippocampal (n = 19) nerve terminals representative of 8 coverslips from 3 synaptosome preparations and 4 coverslips from 1 culture.

(Bergsman and Tsien, 2000; Blaustein et al., 1972), we wanted to be sure that plated synaptosomes retained depolarization-dependent exo-endocytotic vesicular cycling. We used the dye FM 1-43 to measure high [K^+]-evoked vesicle turnover. Most of the plated material was stained following treatment with 45 mM K^+ and 4 μM FM 1-43 (90 s) and a wash in Ca^{2+}-free Tyrode (15 min) (Figure 1A, left and middle), indicating that depolarization stimulated endocytosis in the majority of the nerve terminals. Quenching with 50 μM sulforhodamine ensured that staining was confined to intact structures (Pyle et al., 1999). Following two bouts of exposure to high K^+ (90 mM), the level of fluorescence fell sharply, consistent with significant exocytosis and escape of FM dye (Figure 1A, right). The time course of destaining was similar to that of presynaptic terminals in hippocampal neuron cultures (Figures 1B and 1C; Ryan et al., 1996), indicating that plated synaptosomes displayed intact exo-endocytotic vesicular cycling in response to depolarization.

Electron microscopy was used to determine the composition of the plated clusters (Figure 2). The clusters contained numerous intact presynaptic nerve terminals, defined as closed membrane structures containing small, clear synaptic vesicles. The nerve terminals often had mitochondria (Figures 2A–2C and 2F) and occasional active zones (Figures 2E and 2F). In addition to intact nerve terminals, the clusters contained other structures such as membrane fragments. However, in the smaller clusters the vast majority of the structures were intact nerve terminals. We found that the fractional contribution of intact nerve terminals to the total cluster area was inversely related to the size of the cluster (Figures 2A–2D, p < 0.001, n = 26), increasing to ~80% in clusters ~2 μm in diameter (Figure 2D). Thus, by selecting smaller clusters, we increased the chances of recording from intact nerve terminals. The likelihood that recordings were from nerve terminals was enhanced by the observation that the median diameter of the nerve terminals was significantly larger than the diameter of nonterminal structures, defined as those elements without vesicles (respectively, 0.42 μm, n = 292 terminals versus 0.23 μm, n = 677 in 26 clusters, p < 0.001, Kolmogorov-Smirnov test). The nonterminal structures would probably be too small relative to the pipette opening to allow routine gigaseal formation.

We also measured the number of presynaptic terminals associated with postsynaptic material. Only 5% (14/292) of nerve terminals in the plated synaptosome preparation had associated postsynaptic densities facing active zones. Most (11/14) of these synapses consisted of nerve terminals with apparently intact postsynaptic fragments (Figure 2E, arrow), while the remainder (3/14) had disrupted partial postsynaptic membrane (Figure 2F, arrow). Thus, on morphological grounds, recordings from the postsynaptic elements of these synapses were highly unlikely. Electrophysiological experiments provided further tests of this conclusion. We reasoned that chance recordings from postsynaptic elements would either be in a cell-attached configuration (postsynaptic receptors facing the pipette lumen) or with the patch pipette adhering to the intracellular face of a postsynaptic fragment (receptors facing the bath). Following pipette or bath application of glutamate or aspartate (0.1–1 mM), single channel openings were never observed, weighing against the idea that recordings were made from postsynaptic membranes. Taken together, these data indicated that by focusing on the smaller clusters of the plated synaptosome preparation, it was possible to study neocortical presynaptic terminals with intact vesicle turnover.

Ion Channel Recording in Synaptosome Patches

Electrophysiological recording from synaptosomes was facilitated by use of patch electrodes of high resistance (20–40 MΩ). Inside-out patches were produced by first forming a cell-attached patch, then withdrawing the electrode tip before transiently removing it from the bath solution (Hamill et al., 1981). A cytoplasmic bridge was often observed during withdrawal of the electrode tip. To investigate the quality of recording, we characterized some of the most recognizable channel activity present. Potassium channel currents were often recorded, as exemplified by single channel openings of large conductance, Ca²⁺-activated potassium (BK) channels (Figure 2G). BK channels are known to exist in presynaptic nerve endings (Bartschat and Blaustein, 1985; Sun et al., 1999) and provided an opportunity to validate the patch clamp recordings from synaptosomes. Figures 2G–2I illustrate data from an inside-out patch where the elementary events displayed a unitary conductance of 230 pS and reversal potential (E_r) of −1 mV with 155 mM KCl on both sides of the membrane (Figure 2H). (In all figures, the recording configuration is noted by the inset icon and membrane voltages are described using the convention of intracellular potential minus extracellular potential [inside-out recordings] or membrane voltage relative to the resting potential [synaptosome-attached recordings].) In this patch, reducing bath (cytoplasmic) [K⁺] to 4 mM shifted E_r to +64 mV and reduced the conductance to 80 pS, consistent with the channel being highly K⁺ selective. Analysis of consecutive 500 ms current sweeps revealed that the probability of channel opening (nP_o) in the same patch increased when the [Ca²⁺] on the cytoplasmic side was increased from 1 to 100 μM (Figure 2I). This combination of properties securely identified the channel as BK and verified that we were able to record currents with good control of membrane voltage and intracellular ion concentration.

## Reducing [Ca²⁺]ₒ Activates an Outward Current in Synaptosomes

The effects of reductions in [Ca²⁺]ₒ on ion channel activity at the nerve terminal were first studied in synaptosome-attached recordings (Figure 3). Unless otherwise noted, the patch electrode was filled with standard Tyrode solution containing 2 mM Ca²⁺ and Mg²⁺. Figure 3A illustrates a representative recording with 6 mM Ca²⁺ and no Mg²⁺ in the bath (middle trace), in which we observed no channel activity with a wide range of voltage steps (every 20 mV between −60 and 200 mV). Unexpectedly, when the bath solution [Ca²⁺] was lowered to 60 μM (lower trace), depolarization evoked a smoothly rising outward current that grew progressively larger in amplitude with steps ≥40 mV above the resting potential. This prominent current response was typical of that seen in >85% of the 332 patches when depolarized in lowered [Ca²⁺]ₒ. The response was similar whether the predominant cation in the pipette solution was Na⁺ or K⁺. No response to a decrease in bath [Ca²⁺] was seen in the somata of cultured cortical neurons or acutely dissociated sympathetic neurons, indicating this current change was specific to nerve terminals (W.Y. Chen and S.M.S., unpublished observations). Figure 3B provides another illustration of the slowly developing

outward current, notable because the smoothly increasing current response was surmounted with clear-cut unitary channel openings of BK channels in some of the traces. The BK openings were evoked by a +150 mV pulse, strong enough to activate BK channels even with low cytosolic Ca²⁺ (Cox et al., 1997). With the same test pulse, BK openings were not seen in this recording when the bulk solution was Na-Tyrode with 2 mM Ca²⁺ and Mg²⁺, but only if the bulk [K]ₒ was elevated (35–155 mM, see Figure 3B). The set of results was consistent with a [K]ₒ-sensitive resting potential, as expected for an intact synaptosome. This was corroborated by variations in unitary current amplitude with different values of bulk [K]ₒ. The low background noise, the crispness of the openings and closings, and the constant amplitude of the unitary events indicated the quality of the patch clamp recording (Hamill et al., 1981) and provided reassurance that significant ion accumulation or depletion had not occurred, despite the small volume of the synaptosome.

Divalent Cation Dependence of Activation

Variations in [Ca²⁺]ₒ are known to affect membrane conductances of excitable cells and are generally interpreted in terms of changes in membrane charge screening (Frankenhaeuser and Hodgkin, 1957; Hille, 2001). Typically, a decrease in [Ca²⁺]ₒ from 5 to 0 mM shifts the conductance-voltage curve by $\sim$−30 mV. This explanation is not applicable to the currents in Figure 3 because the Ca²⁺ was reduced outside of the synaptosome, but not within the patch pipette solution directly facing the membrane patch that generated the outward current. Negligible solution exchange between these compartments would be allowed by the high resistance (>2 GΩ) seal surrounding the membrane patch. Even in the unlikely case of complete equilibration between the bathing solution and the medium outside the patch, the observed differences in channel activation would have required a negative voltage shift >180 mV, 6-fold larger than the charge screening effect. Thus, we conclude that the regulation of the outward current must involve some form of modulation that involves external divalent cations but not direct charge screening.

To characterize the dependence of the depolarization-activated outward current on the bulk [Ca²⁺]ₒ, further experiments were carried out in synaptosome-attached patches with divalent cation concentrations held fixed at 2 mM Ca²⁺ and Mg²⁺ in the pipette solution. In the absence of bulk Mg²⁺, the novel outward current was strongly and reversibly decreased by elevations of bulk [Ca²⁺]ₒ in the submillimolar range (Figure 4A). Likewise, in the absence of bulk Ca²⁺, elevations of bulk Mg²⁺ concentration reduced the current (Figure 4B). The IC_{50} values for bulk [Ca²⁺]ₒ and [Mg²⁺]ₒ were 265 ± 64 μM (n = 6) and 761 ± 100 μM (n = 6), respectively (Figure 4C), with Hill coefficients of 1.3 ± 0.1 and 1.2 ± 0.1. With these IC_{50}s, activation of the novel current would increase linearly with modest drops in divalent cation concentration below their normal physiological levels. These values may underestimate the true IC_{50} and physiological activity, as the [Ca²⁺] and [Mg²⁺] in the pipette solution, closest to the ionic pathway itself, were not decreased from their high levels of 2 mM each.
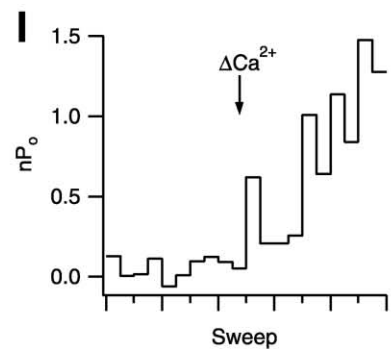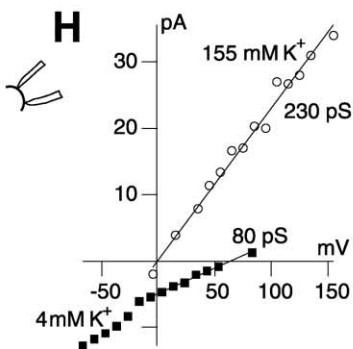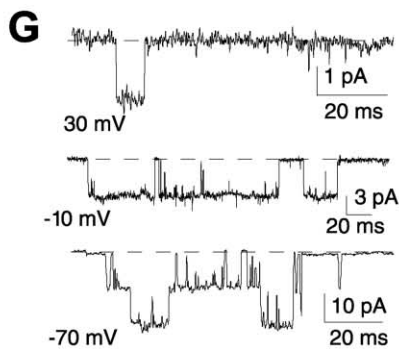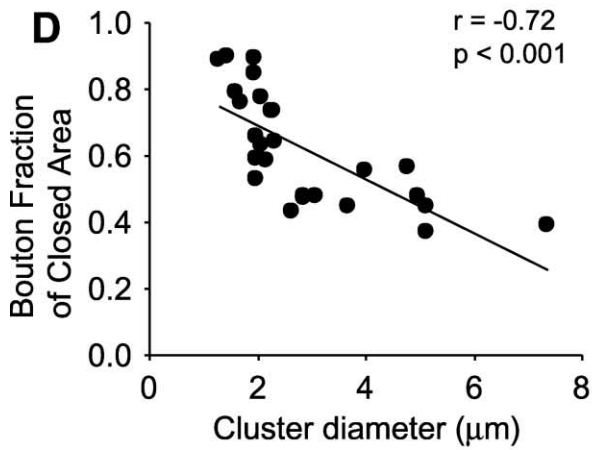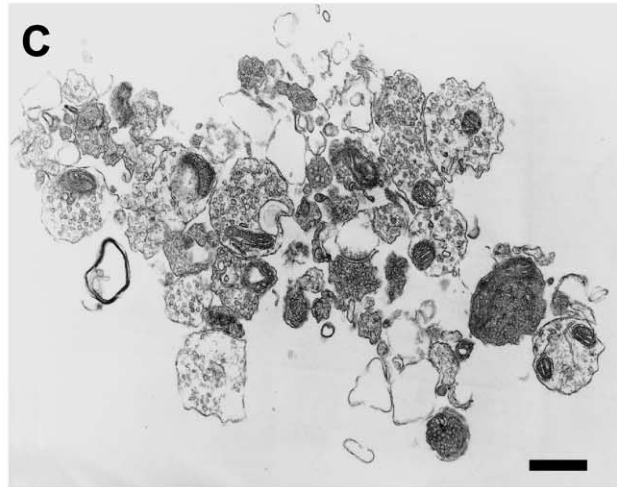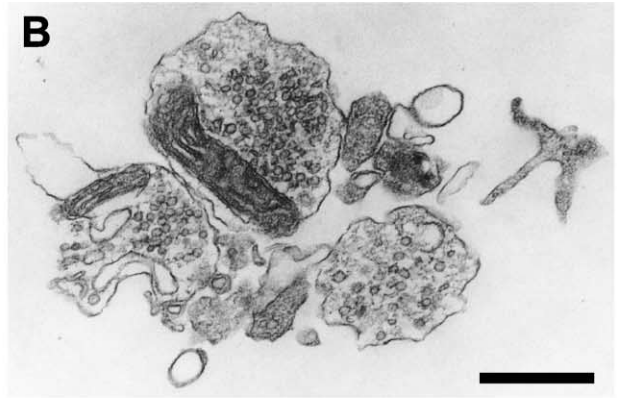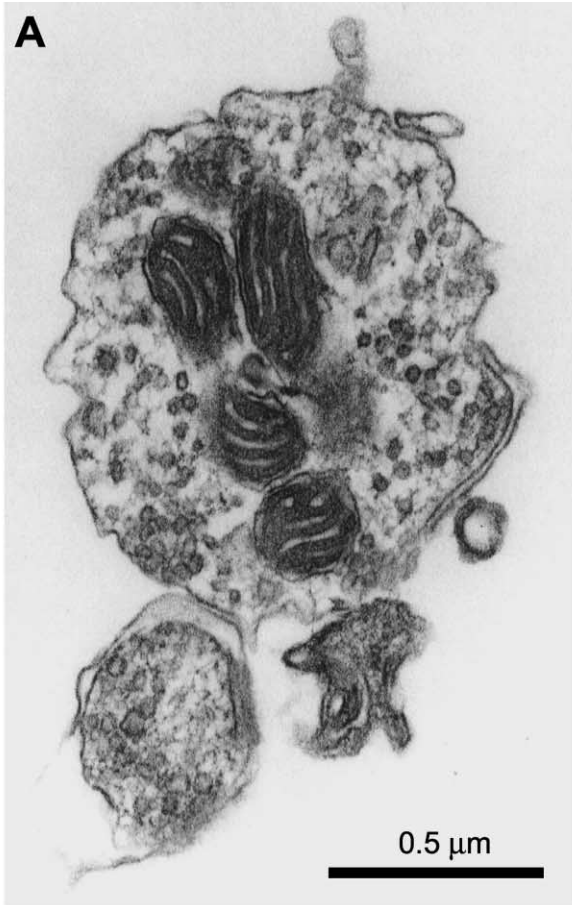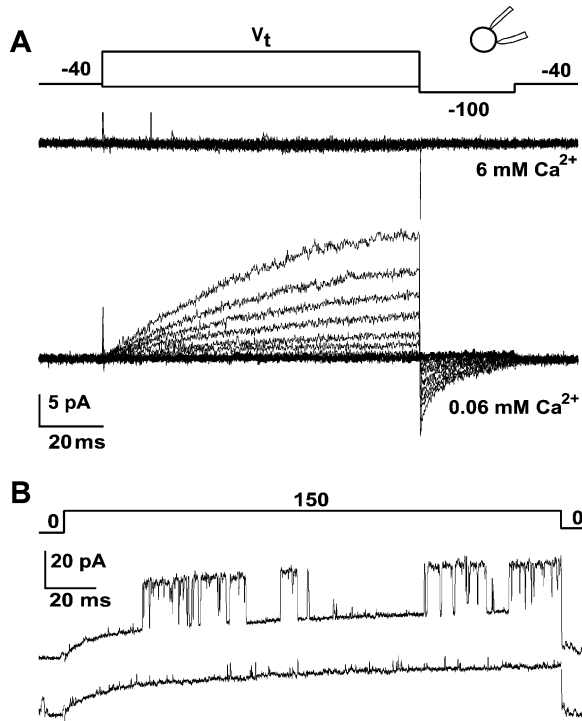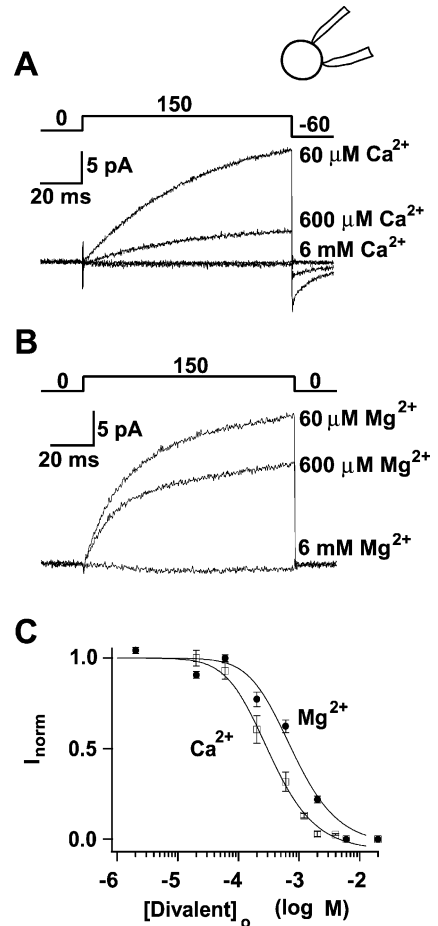
Figure 3. Activation of a Novel Outward Current in Nerve Terminals

(A) Families of outward currents activated by step depolarizations (upper trace) to Vt (every 20 mV between −60 and 200 mV) with 6 mM Ca^{2+} in bath (middle trace) and between −60 mV and 140 mV with 60 μM Ca^{2+} in the bath (lower trace). Bath solution was Tyrode with no divalents except as indicated. Inset: this icon in any figure indicates synaptosome-attached patch configuration.

(B) Outward current surmounted by BK channel openings following a 150 mV depolarization from resting potential in 10 μM Ca^{2+}. Bath solution in this experiment was (in mM) 75 KCl, 150 sucrose, 0.01 CaCl$_2$, 10 HEPES, and 10 glucose.

A Single Conductance System with Voltage-Dependent Kinetics of Activation

Reductions in bulk [Ca^{2+}]$_o$ induced an inward tail current at negative potentials as well as the slowly developing outward current at strongly positive potentials (Figure 3A). To investigate whether inward and outward currents were both generated by a single underlying conductance change, or were the results of kinetically distinct channel types, we utilized an envelope test (Matteson and Armstrong, 1986). In this protocol (Figure 5A), the synaptosome-attached patch was depolarized to +90 mV, then stepped back to −110 mV at various times,
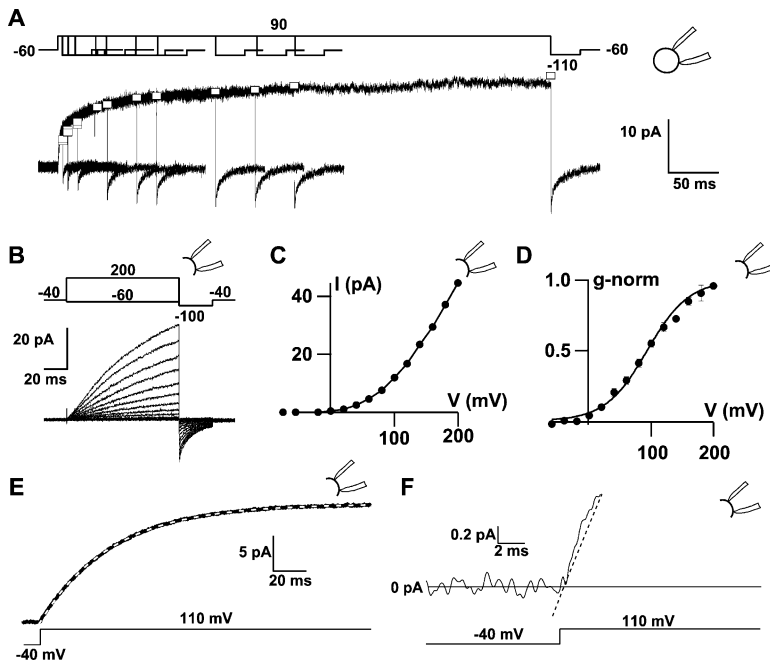

Figure 4. Divalent Cation Dependence of Activation of Outward Current in Nerve Terminals

(A and B) Currents evoked by 150 mV depolarizations from the RP (as indicated by voltage trace [top]), in various [Ca^{2+}]$_o$ (A) or [Mg^{2+}]$_o$ (B). The two high Ca^{2+} traces bracketed the lower Ca^{2+} traces in time.
(C) Concentration-effect curves for Ca^{2+} (open square) and Mg^{2+} (closed circle).

Bath solution was Tyrode with divalents as indicated.

allowing the activation kinetics of the outward current to be compared with that of the inward tail current. There was a good match between the time course of outward current development and that of peak inward tail current (scaled tail current denoted by open squares). These results supported the idea that the outward current and inward tails were both generated by a single conduc-

---

Figure 2. Electron Microscopy and Electrophysiology of Plated Synaptosomes

(A–C) Representative electron micrographs obtained from small- (A), middle- (B), and large- (C) sized clusters.

(D) Proportion of area occupied by nerve terminals to area occupied by all closed structures. A solid line represents linear regression to the data (r = −0.72, p < 0.001, n = 26 clusters). Note that proportion approaches 90% for appropriately small clusters.

(E and F) Representative electron micrographs of synapses within plated synaptosomes. Postsynaptic components were putatively intact (E, arrow) or broken (F, arrow). All scale bars represent 0.5 μm.

(G) Examples of single BK channel openings with 4 mM K$^+$ and 2 mM Ca^{2+} in the bath. Dashed lines indicate zero current level. Inset: this icon in any figure indicates inside-out patch configuration. All voltages described in the paper are absolute membrane voltages (inside-out recordings) or membrane voltage relative to the resting potential ("RP"; synaptosome-attached).

(H) Current-voltage characteristics of single channel openings with 4 mM (closed square) or 155 mM K$^+$ (open circle) in the bath.

(I) Channel open probability (nP$_o$) in consecutive 500 ms sweeps at −10 mV (up to 4 channel openings). At arrow, bath [Ca^{2+}] was increased from 1 μM to 100 μM. G-I from the same recording.

Figure 5. Voltage- and Time-Dependent Kinetics of NSC Activation

(A) Envelope test demonstrates that outward currents and inward tail currents are supported by a single conductance system. Duration of depolarization to 90 mV was varied and the tail currents were recorded at −110 mV in this synaptosome-attached recording. The tail current amplitudes, all scaled by the same factor (open square), superimpose onto the outward currents. The bath contained 155 mM KCl, 10 mM HEPES, and 1 μM CaCl$_2$.

(B) Family of currents activated by depolarizing pulses to levels varied in 20 mV steps between −60 and 200 mV.

(C) Voltage dependence of the peak outward currents in (B).

(D) Normalized conductance-voltage plot obtained by measuring tail current amplitudes in four experiments. Continuous curve is a Boltzmann function with parameters set at means of those obtained in the individual experiments.

(E) Average of 10 currents (upper trace) evoked by a step from −40 mV to +110 mV (lower trace). Overlying the current trace is an exponential fit (dashed white line) to all but the first 5 ms of the depolarization, extrapolated back to the baseline current level.

(F) Expanded view of (E) showing minimal delay in current activation after the depolarizing step (fit is dashed black line).

(B–F) Bath solution was Tyrode with 0.06 mM CaCl$_2$ and 0 mM MgCl$_2$.

tance system whose E_r remained fixed throughout the depolarization. The voltage dependence of activation of the slowly developing conductance was studied in inside-out patches, a recording configuration that allowed rigorous control of the potential and permeant ion concentration on both sides of the membrane (Hamill et al., 1981). Even in this condition, decreases in bulk [Ca^{2+}]$_o$ remained effective in activating the conductance, perhaps because the bulk divalent concentration could be sensed by an annulus of membrane extending beyond the rim of the patch pipette. Slowly developing outward currents were activated increasingly strongly with depolarizations beyond 0 mV (Figures 5B and 5C). Upon repolarization to −100 mV, the inward tail currents deactivated with a time constant of 12 ± 1 ms (n = 4). Analysis of tail currents was used to assess the degree of activation as a function of test potential (Figure 5D). Activation began to saturate at very strongly positive potentials. The half-maximal activation voltage averaged 93 ± 3 mV, and the steepness parameter 34 ± 2 mV. Unitary openings of the outward current were not resolved in the inside-out configuration, just as found in synaptosome-attached recordings, indicating that the single channel conductance was small.

To appreciate better the effect of the current during briefer depolarizations, we examined the kinetics of current activation on a rapid time scale. Depolarization of an inside-out membrane patch in 60 μM bath Ca^{2+} resulted in a time course of current activation that was well fit with a single exponential (Figure 5E). Voltage-gated ion channels often begin to open after a measurable delay due to transitions between closed states leading up to an open state. Extrapolation of the fit back

to the baseline current level indicated little or no delay (<0.32 ms in this example) (Figure 5F).

Ionic Basis of the Outward Current

We studied the ionic basis of the slow current by performing measurements of E_r in inside-out patches (Figure 6). Following an activating depolarization, tail currents were evoked by sudden repolarizations to a range of test potentials on either side of E_r (Figure 6A). As the test potential became increasingly negative, the tail currents underwent a smooth transition from decaying outward to decaying inward (Figure 6B). The E_r was −9 ± 3 mV (n = 5) with symmetrical 150 mM Na$^+$ (Figure 6C). With 155 mM K$^+$ on the intracellular side and 150 mM Na$^+$ and 4 mM K$^+$ on the extracellular side, comparable to normal physiological conditions, E_r was −1 ± 1 mV (n = 3). A Na$^+$:K$^+$ permeability ratio (P$_{Na}$/P$_K$) of 1.4 was calculated from this 8 mV shift (E$_\Delta$) using the difference between the respective Goldman-Hodgkin-Katz equations (E$_\Delta$ = (RT/F)·ln{P$_{Na}$[Na$^+$]$_i$/P$_K$[K$^+$]$_i$}) (Hodgkin and Katz, 1949). When NaCl on the intracellular side was increasingly replaced with isotonic sucrose, E_r was shifted to more positive potentials (Figure 6C). In pooled data from the same five recordings, E_r varied systematically with [Na$^+$]$_i$, increasing by 54 mV per 10-fold reduction of cytoplasmic NaCl (Figure 6D), consistent with permeability to Na$^+$ and not Cl$^−$. In separate inside-out recordings, E_r was unchanged by replacement of bath Cl$^−$ with gluconate (−4 ± 3 mV) or NO$_3^{2−}$ (0.7 ± 0.4 mV), confirming that the currents were generated by a cation channel. Increasing the pipette [Ca^{2+}] to 5 or 10 mM shifted the E_r negatively by up to 4 mV, suggesting no permeability to Ca^{2+}. Overall, these results indicated
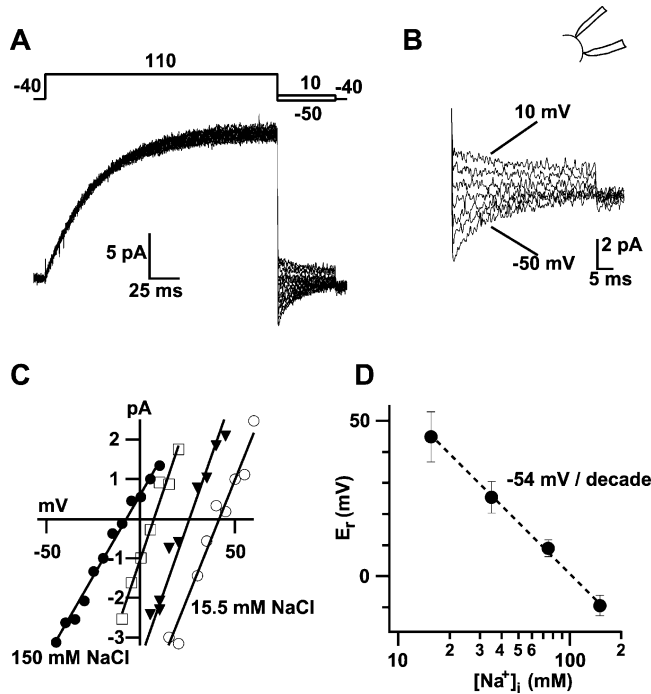
Figure 6. The $[Ca^{2+}]_o$-Modulated Current in Nerve Terminals Is Supported by a Nonselective Cation Channel

(A) Family of currents associated with depolarization to 110 mV and repolarization to potentials from 10 to −50 mV in 10 mV steps. Inside-out patch with nominally Mg^{2+}-free Tyrode solution plus 60 μM Ca^{2+} in the bath.
(B) Tail currents from (A) expanded.
(C) Peak tail current amplitudes (from same patch as A) plotted against tail current voltage recorded in 150 mM (closed circle), 75 mM (open square), 35 mM (closed down triangle), and 15.5 mM (open circle) NaCl. NaCl was substituted isotonically with sucrose.
(D) Plot of E_r versus bath $[Na^+]$. Line shows best fit to average data from five inside-out patches and has a slope of −54 mV/decade.

that a nonselective (monovalent) cation (NSC) channel was responsible for generating the voltage-sensitive outward current.

Mechanism by which $[Ca^{2+}]_o$ Reduction Activates the NSC Channel

The mechanism by which reduction of bulk $[Ca^{2+}]_o$ activates the slow conductance change must be an indirect one, because the gigaseal in the synaptosome-attached configuration prevented Ca^{2+} in the bath from directly affecting the channels bounded by the electrode tip. This sharply distinguishes this NSC channel from NSC channels in neuronal cell bodies that are directly activated by changes in $[Ca^{2+}]_o$ (Hablitz et al., 1986; Xiong et al., 1997). Among possible indirect mechanisms, we considered the possibility that reductions in bath $[Ca^{2+}]$ might act through secondary changes in intrasynaptosomal free Ca^{2+}. We rejected this hypothesis for four reasons. First, synaptosomes are known to be able to maintain low $[Ca^{2+}]_i$ in the absence of overt depolarization (Bergsman and Tsien, 2000; Blaustein et al., 1972; Nachshen, 1985). Second, even in the absence of bulk Ca^{2+}, the NSC channel activity was suppressed by bulk Mg^{2+} (Figure 4B), over a range of $[Mg^{2+}]_o$ known to have little effect on intraterminal $[Mg^{2+}]_i$ (Kennedy, 1998). Third, Gd^{3+} and spermidine modulate the channel in the absence of bulk Ca^{2+}. Finally, synaptosome-attached recordings showed that the dependence of E_r on bulk cation concentration in this configuration was much attenuated compared to that in inside-out recordings. Thus, we could be confident that free mixing between the bath and intracellular compartment did not occur.

We turned to indirect membrane signaling mechanisms as a possible explanation for how lowering divalent ion concentrations in the bath might cause activation of ion channels in the membrane patch bounded by the electrode tip. Like those described here (Figure 4), responses to extracellular Ca^{2+} and Mg^{2+} in the low millimolar range are hallmarks of the Ca^{2+} receptor (CaR), originally identified by Brown and colleagues as the receptor controlling homeostasis of serum $[Ca^{2+}]$ (Brown et al., 1993). For clarity we refer to this as the "CaR" and to the $[Ca^{2+}]_o$-detecting entity in our studies as a "Ca^{2+} sensor". A 7-transmembrane receptor, the CaR has been found in numerous mammalian tissues including brain (Brown and MacLeod, 2001). Immunochemical studies with anti-CaR antibodies revealed a punctate pattern of staining consistent with a presynaptic distribution of CaR (Ruat et al., 1995). In addition to Ca^{2+} and Mg^{2+}, the CaR is activated by Gd^{3+} and polycations such as spermidine (Brown and MacLeod, 2001). Accordingly, these agents were tested on the NSC current in synaptosome-attached recordings (Figure 7A). Gd^{3+} potently inhibited the current, with an IC_{50} of 5 ± 1 μM (n = 6). Spermidine was only slightly less potent, exhibiting an IC_{50} of 12 ± 1 μM (n = 6). Thus, the rank order of potency of polycations was Gd^{3+} > spermidine > Ca^{2+} > Mg^{2+}, which agrees perfectly with the rank order reported previously for the CaR. On the other hand, 0.1–30 μM NPS R-467, an allosteric regulator of the CaR in some but not all cell types (Fox et al., 1999), had no effect at various $[Ca^{2+}]$ (0.06–6 mM; n = 5; Figures 7B and 7C). A sensitivity to Ca^{2+}, a resistance to NPS R-568 (a CaR allosteric agonist), and altered responsiveness to polyvalent cations has been reported for other tissues (Mailland et al., 1997), indicating the existence of $[Ca^{2+}]_o$ sensors that are not identical to the CaR (Hinson et al., 1997), although they may be related.

The CaR is known to signal via G proteins (Brown et al., 1993). This raised the question of whether a membrane-
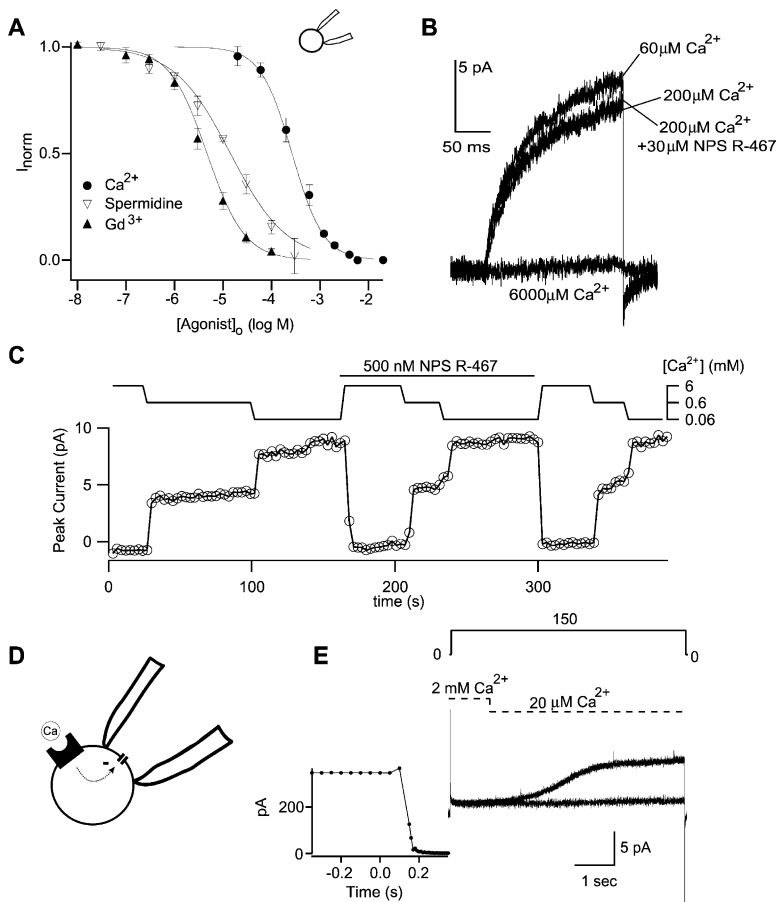
A

I_{norm}

[Agonist]$_o$ (log M)

- Ca^{2+}
- ▽ Spermidine
- ▲ Gd^{3+}

B

5 pA

50 ms

60 μM Ca^{2+}

200 μM Ca^{2+}

200 μM Ca^{2+}
+30 μM NPS R-467

6000 μM Ca^{2+}

C

500 nM NPS R-467

[Ca^{2+}] (mM)

6
0.6
0.06

Peak Current (pA)

time (s)

D

Ca

E

150

0   0

2 mM Ca^{2+}

20 μM Ca^{2+}

pA

200

0

-0.2   0.0   0.2

Time (s)

5 pA

1 sec

Figure 7. Characterization of Ca^{2+} Signaling Mechanism

(A) Concentration dependence of inhibition by Gd^{3+} ($IC_{50} = 5 \pm 1$ μM) and spermidine ($IC_{50} = 12 \pm 1$ μM) in the presence of 60 μM Ca^{2+}. Ca^{2+} data are repeated from Figure 4C for comparison.

(B) NSC channels are not modulated by NPS R-467. Synaptosome-attached currents following 150 mV step depolarizations from RP −40 mV in the presence of 200 μM Ca^{2+} were not affected by addition of 30 μM NPS R-467. Currents activated in presence of 60 μM and 6 mM Ca^{2+} shown for comparison.

(C) Peak outward currents in response to 100 ms steps to 150 mV given every 3 s, regulated by [Ca^{2+}]$_o$ (upper trace) but not NPS R-467 (solid bar) in a synaptosome-attached recording.

(D) Schematic diagram showing separation of the [Ca^{2+}]$_o$ sensor and the channel it inhibits.

(E) NSC channel current (upper current record) evoked by lowering Ca^{2+} (dashed trace) during a sustained 150 mV depolarization from the RP (top). Lower record shows current signal in the absence of a Ca^{2+} change. These currents were not leak subtracted. Inset shows typical temporal response of solution application system measured with repetitive test pulses during solution change from NaCl to water (initiated at t = 0). Bath solution was Tyrode with polyvalents as indicated.

associated second messenger, such as a G protein, is involved in signaling between Ca^{2+} sensors facing the bulk solution and NSC channels in the synaptosome-attached patch (Figure 7D). As a first step toward resolving this issue, we examined the kinetics of the signaling from the Ca^{2+} sensors to the NSC channels within the patch. If [Ca^{2+}]$_o$ were detected by a receptor coupled to a diffusible message, there might be a measurable delay between reduction of bulk [Ca^{2+}]$_o$ and the activation of the NSC channels. Upon reduction of Ca^{2+} from 2 mM to 20 μM (change completed within 200 ms; Figure 7E, inset), at a sustained depolarization, activation of the NSC channel commenced with a lag of ∼450 ms and reached 90% of maximum in 3.2 s (Figure 7E). This time course was an order of magnitude slower than the solution change or voltage-dependent activation at a fixed [Ca^{2+}] and [Mg^{2+}]. The delay was consistent with the lateral diffusion of a membrane-delimited signal. More rapid signaling would be expected under circumstances in which the sensors and channels were not artificially separated by a patch pipette.

Taken together, our data suggest an overall similarity between the signaling mechanism in nerve terminals and in other tissues displaying the CaR, but leave open the question of whether the nerve terminal Ca^{2+} sensor is the CaR, a variant thereof, or a completely different entity.

Activation of the NSC Channel by Physiological Stimuli

When maximally activated, the NSC channel generated a sizeable current in comparison to the surface area of a membrane patch (∼0.14 μm^2 for a 30 MΩ patch pipette; Sakmann and Neher, 1995). When referred to the corresponding capacitance (1.4 fF), a current of 20 pA would generate the high rate of voltage change of ∼14,000 V/s. While currents of this size were frequently recorded, they reflect a near-maximal activation of the NSC pathway, achieved in our recordings by imposing wide variations in membrane potential and external divalent cation concentration. This biophysical analysis does not determine if the NSC channels at presynaptic endings are sufficiently turned on under physiological or pathophysiological conditions to have a significant functional impact.

In one series of experiments, we tested the effects of limited excursions in extracellular divalent ion concentrations, starting from the basal values of 1.1 mM Ca^{2+} and Mg^{2+} found in the brain (Hansen, 1985; Nilsson et al., 1993; Zhang et al., 1990). Figures 8A and 8B illustrates a representative experiment, in which the cell-attached patch and the bulk of the synaptosome were both exposed to Tyrode with 1.1 mM Ca^{2+} and Mg^{2+}. Depolarizations of the synaptosome-attached patch evoked small but clearly defined currents that were approximately 20% of the near-maximal current (Figure 8B).
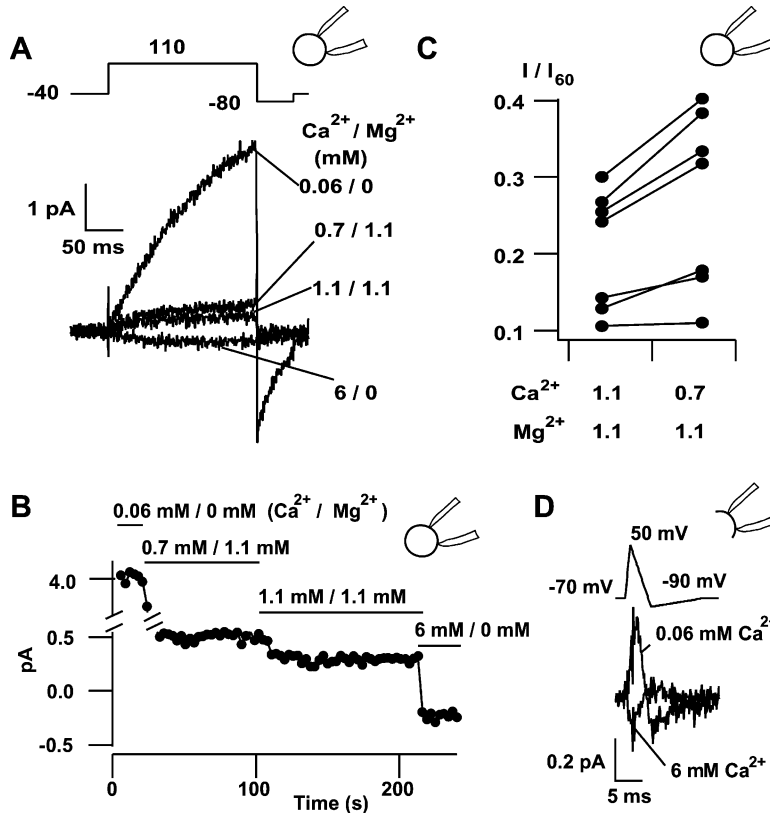
Figure 8. NSC Channel Currents under Near-Physiological Conditions

(A) Comparison of minimal and near maximal NSC currents activated by 110 mV depolarizations with currents activated at physiological $[Ca^{2+}]_o$ and $[Mg^{2+}]_o$.

(B) Peak outward currents plotted against time following changes in divalent cation concentration (indicated by bars) in synaptosome-attached recordings.

(C) Plot of the ratio of peak current to near-maximal current activated in the presence of 60 μM Ca^{2+}_o and no Mg^{2+}. Decreasing $[Ca^{2+}]_o$ in the presence of constant 1.1 mM Mg^{2+} resulted in increased current in all seven experiments.

(D) Calcium dependence of average currents activated by action potential waveforms in the inside-out configuration (n = 300–360). Bath solution was Tyrode with no divalents except as indicated. The pipette solution was Tyrode with 1.1 mM Ca^{2+} and 1.1 mM Mg^{2+}; with 1 μM TTX in (D).

With $[Mg^{2+}]_o$ fixed at 1.1 mM, the current was increased by 29% ± 5% (n = 7; p = 0.005 by paired t test) (Figure 8C) when $[Ca^{2+}]_o$ was 33% lower, a conservative estimate for the decline during moderate activity (Nicholson et al., 1978; Stanley, 2000). Even larger drops in cleft $[Ca^{2+}]_o$ and greater activation of NSC channels would be expected if opening of Ca^{2+} permeable ligand-gated channels in the postsynaptic membrane were also taken into account. These data probably underestimated the impact of changing global $[Ca^{2+}]_o$, since the bath $[Ca^{2+}]_o$ was lowered without altering the $[Ca^{2+}]_o$ in the pipette solution directly apposed to the channels, which would be expected to give the closest and strongest stimulus for activation. This hypothesis is supported by a comparison of Figure 4C to 8C. Reduction of the Ca^{2+} and Mg^{2+} in the pipette solution from 2 mM to 1.1 mM increased the relative amplitude of the currents seen with 1.1 mM Ca^{2+} in the bath despite the presence of bath Mg^{2+} in the latter experiment.

A second series of experiments tested whether the NSC channel activated quickly enough to contribute membrane currents during and following individual action potentials. Figure 8D shows currents evoked by action potential waveforms (APWs) applied to an inside-out patch. With lowered $[Ca^{2+}]_o$ in the bathing solution, we observed a biphasic current (an outward and then inward component) that was not seen with elevated $[Ca^{2+}]_o$. The NSC channel activation with millisecond depolarizations was consistent with their strictly first order kinetics of activation (Figure 5E). During the application of 30 APWs (30 Hz) at a constant $[Ca^{2+}]_o$, the

amplitude of the NSC currents did not fall off with time ($30^{th}/1^{st}$ = 1.01 ± 0.12), consistent with the observed lack of inactivation. Together these data suggest that the Ca^{2+} sensor-NSC channel pathway may be activated at resting $[Ca^{2+}]_o$ and slowly responds to decreases in cleft $[Ca^{2+}]$.

Discussion

The concept that presynaptic terminals might sense and respond to changes in cleft $[Ca^{2+}]$ was first postulated more than a decade ago (Smith, 1992). We have now described a new pathway through which decreases in $[Ca^{2+}]_o$ may be transduced to changes in presynaptic membrane properties. Our experiments led us to several unexpected findings. First, neocortical nerve terminals can be directly approached with patch clamp recordings. Second, the terminals prominently display a NSC conductance that is jointly activated by reductions in $[Ca^{2+}]_o$ and by membrane depolarization, with novel biophysical properties that distinguish the conductance from channels previously described in neuronal cell bodies. Third, the response to Ca^{2+} does not occur by a direct action on the NSC channel itself, but operates over a distance, with pharmacology reminiscent of the CaR. Fourth, the Ca^{2+} sensor-NSC channel pathway is well suited to transduce changes in cleft $[Ca^{2+}]$ arising from either presynaptic or postsynaptic Ca^{2+} fluxes and may have significant effects on presynaptic electrical activity.

Recordings from Neocortical Nerve Terminals

This is the first electrophysiological study of functional neocortical nerve terminals. It was of considerable interest to apply patch clamp techniques to synaptosomes, a preparation traditionally approachable only with neurochemistry. The plated synaptosome preparation displayed intact vesicle cycling (Figure 1) and included clumps of pinched-off nerve terminals, visualized by EM (Figure 2). We confined our recordings to small synaptosome clumps, made up almost entirely of nerve terminals (Figure 2). The feasibility of patch-clamp recording from these nerve terminals was established by finding appropriate biophysical behavior of BK channels (Figure 2). It will be interesting to compare the electrophysiological properties of cortical synaptosomes with those of larger presynaptic structures such as the calyx of Held (Forsythe, 1994) or mossy fiber terminals (Geiger and Jonas, 2000), or inhibitory terminals of cerebellar basket cells (Southan and Robertson, 1998). Cortical nerve terminals are of special interest because of their abundance and importance for brain function.

Unconventional Aspects of the Ca^{2+} Sensor-NSC Channel Pathway

Here we discuss key properties of the NSC channel and how it might help link local changes in $[Ca^{2+}]_o$ to modification of presynaptic electrical activity.

Nonselective Cation Conductance

The NSC pathway is permeant to Na^+ and K^+ but not Cl^- (Figure 6). Because its E_r is near zero under physiological conditions, the activated NSC channel would provide inward current in nerve terminals at rest. Finding that reductions in $[Ca^{2+}]_o$ specifically activate a distinctive NSC channel supplies a satisfying explanation of previous radiotracer data showing that a reduction in $[Ca^{2+}]_o$ caused synaptosomes to undergo depolarization and increased permeability to Na^+ (Schmalzing, 1985). Much of the depolarization remained even in tetrodotoxin (TTX), suggesting that a pathway other than fast Na^+ channels must be involved (Kauppinen et al., 1986). The features of the NSC conductance are appropriate to account for all these observations. A mild depolarization would favor repetitive firing, possibly explaining increased excitability of cortical neurons upon lowering $[Ca^{2+}]_o$ (Burgo et al., 2003). But steady depolarization may also cause Na^+ channel inactivation and decreased excitability.

Strong Dependence on Decreases in External Ca^{2+} Concentration

Activation of the NSC current takes place over a range of $[Ca^{2+}]_o$ that brackets the variation in cleft $[Ca^{2+}]$ expected under physiological conditions (Figure 4C). In the presence of Mg^{2+}, the current was increased by 29% with a 33% reduction in $[Ca^{2+}]_o$ below basal. It has been estimated that during normal transmission, cleft $[Ca^{2+}]$ could easily drop by >33% because of presynaptic Ca^{2+} influx alone (ignoring postsynaptic Ca^{2+} flux via NMDA receptors). Even greater falls in $[Ca^{2+}]_o$, down to 0.1 mM, have been measured in mammalian brains during disease states (Zhang et al., 1990).

Indirect Mechanism of Modulation

NSC channels within a synaptosome-attached patch could be activated by lowering the divalent cation concentration in the solution outside the pipette. By allowing reproducible activation without any change in the milieu immediately external to the channel, the synaptosome-attached recordings established that, in principle, communication could occur over a distance. The signal could be transmitted by a diffusible factor with an inhibitory action on the NSC channel, produced by Ca^{2+} occupation of its sensor. Alternatively, Ca^{2+} binding could cause destruction of a constitutive factor that tonically activates the channel. Either way, the indirect action of Ca^{2+} differs from well-known direct effects: altered membrane charge screening (Frankenhaeuser and Hodgkin, 1957; Hille, 2001) and binding to state-dependent sites on ion channels (Armstrong and Cota, 1999). The indirect nature of the signaling was corroborated by its delayed time course (Figure 7E). The delay would be shorter if the Ca^{2+} sensor and NSC channel were closer together, as expected for nerve terminals in situ. An indirect mechanism avoids the need for strict colocalization of Ca^{2+} sensors and the downstream conductance: sensors could be concentrated near the cleft, while the channels could be anywhere on the nerve terminal.

Generic Resemblance to the Classical Ca^{2+} Receptor

The Ca^{2+} sensor in synaptosomes displayed several earmarks of the CaR, first isolated from parathyroid by Brown and colleagues (Brown et al., 1993) and later shown to be present in cerebral cortex by immunocytochemistry (Ruat et al., 1995) and in situ hybridization (Rogers et al., 1997). The synaptosomal Ca^{2+} sensor was sensitive to key agonists of CaRs, with a rank order of potency typical of the CaR, Gd^{3+} > spermidine > Ca^{2+} > Mg^{2+}. The IC_{50} values for Ca^{2+} and Mg^{2+} differed by 3-fold (0.26 mM, 0.76 mM), similar in separation to EC_{50} values for the parathyroid CaR (3 mM, 10 mM). The greater sensitivity to polyvalent agents in our experiments might be attributed to differences in the downstream signaling that links Ca^{2+} sensing to the final response. Alternatively, differences in potency might arise from molecular properties in the sensing mechanism itself, in keeping with the insensitivity of the synaptosomal Ca^{2+} sensor-NSC pathway to NPS R-467, a modulator of the CaR (Figures 7B and 7C). The responsiveness to such agents varies greatly across diverse CaR-containing cell types (Fox et al., 1999), consistent with evidence for $[Ca^{2+}]_o$ sensors similar but not identical to the CaR (Hinson et al., 1997). Even single amino acid mutations can abolish sensitivity to CaR allosteric agonists and alter Ca^{2+} affinity (Brown and MacLeod, 2001). Further experiments may reveal whether the Ca^{2+} sensor at nerve terminals is an alternatively glycosylated form of CaR, a different splice variant, a new member of the CaR family, or a completely distinct entity (Brown and MacLeod, 2001). Whatever its explanation, the relatively high Ca^{2+} sensitivity in cortical nerve terminals seems appropriately tuned to the range of $[Ca^{2+}]_o$ that would likely be encountered in synaptic clefts.

Unique Biophysical Properties of the NSC Conductance

The Ca^{2+} sensor-NSC channel pathway in nerve terminals can be readily distinguished from other pathways by which $[Ca^{2+}]_o$ can modulate neuronal excitability, described in neuronal cell bodies. For example, $[Ca^{2+}]_o$ can

modulate novel channels selective for Na^+ (Immke and McCleskey, 2001) or K^+ (Johnson et al., 2001). A nonselective cation channel on hippocampal neuron cell bodies has been linked to the classical CaR (Ye et al., 1997), but unlike the NSC channel in synaptosomes, the somatic channels have a large unitary conductance, show no dependence of conductance on the permeating cation concentration, and are activated (not inhibited) by polyvalent cations. Increases in $[Ca^{2+}]_o$ also inhibited a NSC channel in neuronal somata (Formenti et al., 2001; Hablitz et al., 1986), but that channel had a resolvable single channel conductance and was not voltage dependent (Xiong et al., 1997). Such large-conductance NSC channels were not seen in our recordings. Conversely, the NSC conductance described here was not found in recordings from neuronal cell bodies (W.Y. Chen and S.M.S., unpublished). A characteristic feature of the synaptosomal NSC channel, its very small single channel conductance, may be of advantage for smoothly regulating electrical properties of nerve terminals, avoiding the stochastic appearance of large unitary currents.

Prevalence of NSC Channels on Cortical Synaptic Terminals

A high proportion (>85%) of cortical nerve terminals displayed the NSC current when challenged with a drop in $[Ca^{2+}]_o$. Moreover, NSC currents in membrane patches often reached 20 pA, a very large current when referred to the 0.14 μm^2 patch area expected for 30 MΩ patch electrodes (Sakmann and Neher, 1995). The corresponding conductance, 1.4 nS/μm^2, may reflect the maximal activation of the NSC pathway, achieved by imposition of wide variations in membrane potential and external divalent cation concentration. This is appropriate for biophysical analysis, but greatly exceeds what might be experienced by a nerve terminal in situ. However, we may use our characterization of the divalent cation and voltage dependence of NSC channels to estimate their degree of activation under physiological or pathophysiological circumstances.

Possible Effects on Resting Membrane Potential

This can be assessed by comparison with the basal conductance of mossy fiber terminals, 208 pS for a terminal surface area of 144 μm^2, or ~1.5 pS/μm^2 (Hallermann et al., 2003). If small presynaptic terminals are similar, only a minute fraction of the NSC conductance would need to be activated to modify their electrical activity. Allowing for voltage-dependent regulation of NSC channels by extrapolating their steady-state activation curve to −70 mV, the fractional voltage-dependent activation would be 0.8%. In the presence of 1.1 mM Mg^{2+}, the incremental change in NSC conductance (Δg_{NSCC}) upon lowering $[Ca^{2+}]_o$ from 1.1 to 0.7 mM was ~6% of the maximal conductance (Figure 8); a larger fall in $[Ca^{2+}]_o$, from 1.1 mM to 0.2 mM, produced a Δg_{NSCC} ~20% of maximal (Figure 4). Thus, the predicted changes in NSC conductance at −70 mV would be 0.7 pS/μm^2 [= 1.4 nS/μm^2 × 0.008 × 0.06] or 2.2 pS/μm^2. These predicted conductance changes would exert a significant impact on resting potential when pitted against an estimated resting membrane conductance of ~1.5 pS/μm^2, in keeping with previous data indicating that synaptosomes underwent depolarization and in-

creased Na^+ permeability in response to lowered $[Ca^{2+}]_o$ (Kauppinen et al., 1986; Schmalzing, 1985). This calculation might be conservative in using the degree of activation at −70 mV. The greater the depolarization, the more the activation of NSC conductance—analogous to opening of voltage-gated Na^+ channels, but without counteracting inactivation.

Possible Effects on Presynaptic Excitability

Through depolarization of the resting membrane, NSC channels could exert indirect effects on the presynaptic excitability. Mild depolarizations would facilitate spike initiation and might broaden action potentials by inactivating A-type K^+ channels. Stronger depolarizations might promote inactivation of TTX-sensitive Na^+ channels. The net effect of changes in resting potential would depend on the entire complement of ionic currents in the nerve terminal and nearby axon, but the participation of the NSC pathway would render the membrane potential sensitive to $[Ca^{2+}]_o$.

The NSC channel could be directly activated by individual action potential-like waveforms, as seen in inside-out patch recordings where the absolute membrane potential is certain (Figure 8D). The ability of NSC channels to turn on with millisecond depolarizations is in accord with their first-order kinetics of activation (delay <350 μs): might they exert feedback effects on action potential configuration? Because their E_r is near zero, the NSC channels would supply outward current to hasten early repolarization, while providing inward current later on to delay the final repolarization. The potential impact of NSC current can be roughly estimated by the relationship $I_i/C_m = -dV/dt$. The observation of a peak inward NSC channel current of 0.4 pA when $[Ca^{2+}]_o$ was 60 μM (Figure 8D) translates to a hypothetically unopposed rate of voltage change of 285 V/s (= 0.4 pA/1.4 fF). A similar calculation yields 71 V/s at 0.7 mM Ca^{2+}. These rates of change of voltage are comparable to naturally occurring rates of AP repolarization, typically ~250 V/s. Thus, the inward NSC current could significantly broaden the spike and thus prolong Ca^{2+} entry (Borst and Sakmann, 1999b). Another possible action would be the reduction of the presynaptic afterhyperpolarization, which would then alter Na^+ channel gating. Thus, possible outcomes of cleft Ca^{2+} depletion and NSC activation include changes in neurotransmission or presynaptic excitability. Unlike presynaptic mechanisms triggered by changes in $[Ca^{2+}]_i$, the sensitivity of the NSC channels to falls in $[Ca^{2+}]_o$ provides a means by which postsynaptic Ca^{2+} influx may exert a retrograde influence on presynaptic activity.

Possible Effect on Neurotransmitter Release Mediated by $[Na^+]_i$

By increasing intraterminal $[Na^+]$, NSC channel activation may increase resting $[Ca^{2+}]_i$, thereby favoring exocytosis upon subsequent Ca^{2+} entry. This may be a potent effect (Mulkey and Zucker, 1992), because release probability is steeply dependent on $[Ca^{2+}]_i$, with an exponent between 3 and 6 (Dodge and Rahamimoff, 1967; Heidelberger et al., 1994), and in turn, $[Ca^{2+}]_i$ is steeply dependent on $[Na]_i$ because the stoichiometry of the Na^+/Ca^{2+} exchanger is 3:1 or 4:1. Thus, NSC activation would provide considerable leverage on neurotransmitter release, like that which digitalis or elevated beat frequency exert on cardiac contractions.

Conclusions

In summary, our experiments bring cortical synaptosomes, a widely used preparation amenable to neurochemistry, into the select group of nerve terminals that can be accessed by patch clamp recordings. The most prominent membrane current was supported by a novel NSC channel. Activation of this current was readily apparent in the great majority of nerve terminals and was jointly favored by presynaptic depolarization and by decreasing $[Ca^{2+}]_o$ over the submillimolar range, through operation of a Ca^{2+} sensor similar, but probably not identical to the CaR. The NSC channel is likely to contribute to depolarizations of presynaptic terminals which may occur as a result of progressive and sustained falls in synaptic cleft $[Ca^{2+}]$ in physiological or pathophysiological settings.

Experimental Procedures

Synaptosomes

Cortical synaptosomes were prepared from one brain resuspended in 2 ml Tyrode after removal of the cerebellum, diencephalon, and hippocampus (Bergsman and Tsien, 2000). Synaptosomes were plated onto coverslips and stored for 0.5–6 hr at 4°C before use. Cortical synapses are mostly excitatory (89%; DeFelipe et al., 2002).

FM 1-43 Fluorimetry

Synaptosomes and hippocampal neurons were stained for 90 s with 4 μM FM 1-43 in 45 mM K$^+$ Tyrode, then washed for at least 15 min. Images were acquired and analyzed using the Fluoview confocal microscope (Olympus America, Melville, NY). Measurements represent absolute fluorescence levels. Background fluorescence in synaptosome experiments was reduced with 50 μM sulforhodamine (Pyle et al., 1999). FM 1-43 was excited at 488 nm and fluorescence emission was measured above 510 nm (and below 550 nm for synaptosomes). Hippocampal cultures were prepared as described (Klingauf et al., 1998).

Electron Microscopy

For electron microscopy, synaptosomes plated on uncoated glass coverslips for 1.5 hr were fixed with 2% glutaraldehyde in 100 mM phosphate buffer for 30 min at 4°C. Thereafter, they were processed in a Pelco 3450 microwave oven (Ted Pella, Redding, CA). They were postfixed in 2% OsO$_4$ in 100 mM cacodylate buffer, en bloc stained with 5% aqueous uranyl acetate, dehydrated in an ethanol series (50%, 70%, 95%, 100%), and infiltrated in EMbed 812 resin (Electron Microscopy Sciences, Fort Washington, PA). Thin sections (50–70 nm) were cut parallel to the coverslip surface and were poststained with 5% aqueous uranyl acetate and Sato's lead citrate. Sections were examined (Philips 410) at 80 kV accelerating voltage.

The diameter of a synaptosome cluster was obtained by averaging the longer and shorter dimensions. The fractional area of closed membrane structures was calculated with a similarly obtained diameter, assuming a circular shape. They were classified as nerve terminals or nonterminals based on the presence or absence of small clear synaptic vesicles.

Solutions

Tyrode consisted of (in mM) NaCl, 150; KCl, 4; HEPES, 10; Glucose, 10; pH adjusted to 7.35 with NaOH. High K$^+$ solutions were made by replacing Na$^+$ with K$^+$. $[Ca^{2+}]$ and $[Mg^{2+}]$ were varied without osmotic compensation. In experiments described in Figures 2 and 3B, HEDTA and Ca^{2+} were added to give a bath $[Ca^{2+}]$ of 1–100 μM in accordance with the Maxchelator program (Bers et al., 1994). In all other experiments, Ca^{2+} and Mg^{2+} were added directly to the solution from concentrated stocks without Ca^{2+} buffers. Liquid junction potentials arising from changes in the bath solution were minimized by use of a 3 M KCl-agar bridge. Bath solutions continuously flowed at 0.5–2 ml/min. Test solutions were applied by gravity from a linear array of glass capillaries under control of a stepper motor. Pipette solution was standard Tyrode with 2 mM CaCl$_2$ and 2 mM

MgCl$_2$ unless otherwise indicated. Experiments were conducted at room temperature (23°C–24°C). Errors and error bars indicate SEM.

Electrophysiology

Recordings were made from isolated nerve terminals visualized on an inverted microscope (Axiovert, Zeiss). Gigaseals (usually 2–30 GΩ) were made with synaptosomes in small clumps (Figure 1). An Axopatch 200A amplifier (Axon Instruments) was used in both synaptosome-attached and inside-out patch-clamp recordings (Hamill et al., 1981). In the synaptosome-attached configuration, the membrane patch and outer cell membrane were in series. The properties of the resulting voltage divider will depend on the patch and bulk membrane areas. A spherical synaptosome of 0.7 μm diameter (see Figure 2) would have a surface area of 1.5 μm². With a patch area of 0.14 μm², the voltage drop across the bulk membrane would be ~10% of the applied voltage, assuming equal specific resistance for both membranes. Both area values may be underestimates. Bulk area, estimated in other nerve terminals from membrane capacitance and a specific capacitance of 1 μF/cm², can exceed the apparent spherical surface area by 2.3-fold (Hallermann et al., 2003). Our estimate of patch area does not allow for an omega-shaped geometry (reasonable because only very mild suction was applied to form the gigaseals). No correction has been made for the voltage divider error, expected only in synaptosome-attached recordings. Pulse Control (4.6 and 5.0) and Igor Pro (3.14) were used to manage data acquisition, storage, and analysis. Currents were prefiltered with a 2 or 5 kHz Bessel filter and digitized at 20–100 μs per point. Leak and capacitative currents were subtracted unless indicated using a −P/4 or −P/8 protocol. Pipette resistances were usually 25–40 MΩ.

Materials

FM 1-43 was from Molecular Probes (Eugene, OR). NPS R-467 was kindly donated by NPS Pharmaceuticals (Salt Lake City, UT). Other reagents were from Fluka (Buchs, Switzerland), Aldrich (Milwaukee, WI), or Sigma (St. Louis, MO).

References

Armstrong, C.M., and Cota, G. (1999). Calcium block of Na+ channels and its effect on closing rate. Proc. Natl. Acad. Sci. USA 96, 4154–4157.

Bartschat, D.K., and Blaustein, M.P. (1985). Calcium-activated potassium channels in isolated presynaptic nerve terminals from rat brain. J. Physiol. 361, 441–457.

Bergsman, J.B., and Tsien, R.W. (2000). Syntaxin modulation of calcium channels in cortical synaptosomes as revealed by botulinum toxin C1. J. Neurosci. 20, 4368–4378.

Bers, D., Patton, C., and Nuccitelli, R. (1994). A practical guide to the preparation of Ca buffers. In Methods Cell Biology (San Diego: Academic Press), pp. 3–29.

Blaustein, M.P., Johnson, E.M., Jr., and Needleman, P. (1972). Calcium-dependent norepinephrine release from presynaptic nerve endings in vitro. Proc. Natl. Acad. Sci. USA 69, 2237–2240.

Borst, J.G., and Sakmann, B. (1999a). Depletion of calcium in the synaptic cleft of a calyx-type synapse in the rat brainstem. J. Physiol. 521, 123–133.

Borst, J.G., and Sakmann, B. (1999b). Effect of changes in action

potential shape on calcium currents and transmitter release in a calyx-type synapse of the rat auditory brainstem. Philos. Trans. R. Soc. Lond. B Biol. Sci. *354*, 347–355.

Brown, E.M., and MacLeod, R.J. (2001). Extracellular calcium sensing and extracellular calcium signaling. Physiol. Rev. *81*, 239–297.

Brown, E.M., Gamba, G., Riccardi, D., Lombardi, M., Butters, R., Kifor, O., Sun, A., Hediger, M.A., Lytton, J., and Hebert, S.C. (1993). Cloning and characterization of an extracellular Ca(2+)-sensing receptor from bovine parathyroid. Nature *366*, 575–580.

Burgo, A., Carmignoto, G., Pizzo, P., Pozzan, T., and Fasolato, C. (2003). Paradoxical Ca2+ rises induced by low external Ca2+ in rat hippocampal neurones. J. Physiol. *549*, 537–552.

Cox, D.H., Cui, J., and Aldrich, R.W. (1997). Allosteric gating of a large conductance Ca-activated K+ channel. J. Gen. Physiol. *110*, 257–281.

DeFelipe, J., Alonso-Nanclares, L., and Arellano, J.I. (2002). Microstructure of the neocortex: comparative aspects. J. Neurocytol. *31*, 299–316.

Dodge, F., Jr., and Rahamimoff, R. (1967). Co-operative action of calcium ions in transmitter release at the neuromuscular junction. J. Physiol. *193*, 419–432.

Egelman, D.M., and Montague, P.R. (1999). Calcium dynamics in the extracellular space of mammalian neural tissue. Biophys. J. *76*, 1856–1867.

Formenti, A., De Simoni, A., Arrigoni, E., and Martina, M. (2001). Changes in extracellular Ca(2+) can affect the pattern of discharge in rat thalamic neurons. J. Physiol. *535*, 33–45.

Forsythe, I.D. (1994). Direct patch recording from identified presynaptic terminals mediating glutamatergic EPSCs in the rat CNS, in vitro. J. Physiol. *479*, 381–387.

Fox, J., Lowe, S.H., Conklin, R.L., Petty, B.A., and Nemeth, E.F. (1999). Calcimimetic compound NPS R-568 stimulates calcitonin secretion but selectively targets parathyroid gland Ca(2+) receptor in rats. J. Pharmacol. Exp. Ther. *290*, 480–486.

Frankenhaeuser, B., and Hodgkin, A.L. (1957). The action of calcium on the electrical properties of squid axons. J. Physiol. *137*, 218–244.

Geiger, J.R., and Jonas, P. (2000). Dynamic control of presynaptic Ca(2+) inflow by fast-inactivating K(+) channels in hippocampal mossy fiber boutons. Neuron *28*, 927–939.

Hablitz, J.J., Heinemann, U., and Lux, H.D. (1986). Step reductions in extracellular Ca2+ activate a transient inward current in chick dorsal root ganglion cells. Biophys. J. *50*, 753–757.

Hallermann, S., Pawlu, C., Jonas, P., and Heckmann, M. (2003). A large pool of releasable vesicles in a cortical glutamatergic synapse. Proc. Natl. Acad. Sci. USA *100*, 8975–8980.

Hamill, O.P., Marty, A., Neher, E., Sakmann, B., and Sigworth, F.J. (1981). Improved patch-clamp techniques for high-resolution current recording from cells and cell-free membrane patches. Pflugers Arch. *391*, 85–100.

Hansen, A.J. (1985). Effect of anoxia on ion distribution in the brain. Physiol. Rev. *65*, 101–148.

Heidelberger, R., Heinemann, C., Neher, E., and Matthews, G. (1994). Calcium dependence of the rate of exocytosis in a synaptic terminal. Nature *371*, 513–515.

Hille, B. (2001). Ion Channels of Excitable Membranes (Sunderland, MA: Sinauer Associates).

Hinson, T.K., Damodaran, T.V., Chen, J., Zhang, X., Qumsiyeh, M.B., Seldin, M.F., and Quarles, L.D. (1997). Identification of putative transmembrane receptor sequences homologous to the calcium-sensing G-protein-coupled receptor. Genomics *45*, 279–289.

Hodgkin, A.L., and Katz, B. (1949). The effect of sodium ions on the electrical activity of the giant axon of the squid. J. Physiol. *108*, 37–77.

Immke, D.C., and McCleskey, E.W. (2001). Lactate enhances the acid-sensing Na+ channel on ischemia-sensing neurons. Nat. Neurosci. *4*, 869–870.

Johnson, J.P., Jr., Balser, J.R., and Bennett, P.B. (2001). A novel

extracellular calcium sensing mechanism in voltage-gated potassium ion channels. J. Neurosci. *21*, 4143–4153.

Kauppinen, R.A., Sihra, T.S., and Nicholls, D.G. (1986). Divalent cation modulation of the ionic permeability of the synaptosomal plasma membrane. Biochim. Biophys. Acta *860*, 178–184.

Kennedy, H.J. (1998). Intracellular Mg2+ regulation in voltageclamped *Helix aspersa* neurones measured with mag-fura-2 and Mg(2+)-sensitive microelectrodes. Exp. Physiol. *83*, 449–460.

Klingauf, J., Kavalali, E.T., and Tsien, R.W. (1998). Kinetics and regulation of fast endocytosis at hippocampal synapses. Nature *394*, 581–585.

Kullmann, D.M., Min, M.Y., Asztely, F., and Rusakov, D.A. (1999). Extracellular glutamate diffusion determines the occupancy of glutamate receptors at CA1 synapses in the hippocampus. Philos. Trans. R. Soc. Lond. B Biol. Sci. *354*, 395–402.

Mailland, M., Waelchli, R., Ruat, M., Boddeke, H.G., and Seuwen, K. (1997). Stimulation of cell proliferation by calcium and a calcimimetic compound. Endocrinology *138*, 3601–3605.

Matteson, D.R., and Armstrong, C.M. (1986). Properties of two types of calcium channels in clonal pituitary cells. J. Gen. Physiol. *87*, 161–182.

Mulkey, R.M., and Zucker, R.S. (1992). Posttetanic potentiation at the crayfish neuromuscular junction is dependent on both intracellular calcium and sodium ion accumulation. J. Neurosci. *12*, 4327–4336.

Nachshen, D.A. (1985). Regulation of cytosolic calcium concentration in presynaptic nerve endings isolated from rat brain. J. Physiol. *363*, 87–101.

Nicholson, C., ten Bruggencate, G., Stöckle, H., and Steinberg, R. (1978). Calcium and potassium changes in extracellular microenvironment of cat cerebellar cortex. J. Neurophysiol. *41*, 1026–1039.

Nilsson, P., Hillered, L., Olsson, Y., Sheardown, M.J., and Hansen, A.J. (1993). Regional changes in interstitial K+ and Ca2+ levels following cortical compression contusion trauma in rats. J. Cereb. Blood Flow Metab. *13*, 183–192.

Nilsson, P., Laursen, H., Hillered, L., and Hansen, A.J. (1996). Calcium movements in traumatic brain injury: the role of glutamate receptor-operated ion channels. J. Cereb. Blood Flow Metab. *16*, 262–270.

Pyle, J.L., Kavalali, E.T., Choi, S., and Tsien, R.W. (1999). Visualization of synaptic activity in hippocampal slices with FM1–43 enabled by fluorescence quenching. Neuron *24*, 803–808.

Rabl, K., and Thoreson, W.B. (2002). Calcium-dependent inactivation and depletion of synaptic cleft calcium ions combine to regulate rod calcium currents under physiological conditions. Eur. J. Neurosci. *16*, 2070–2077.

Rogers, K.V., Dunn, C.K., Hebert, S.C., and Brown, E.M. (1997). Localization of calcium receptor mRNA in the adult rat central nervous system by in situ hybridization. Brain Res. *744*, 47–56.

Ruat, M., Molliver, M.E., Snowman, A.M., and Snyder, S.H. (1995). Calcium sensing receptor: molecular cloning in rat and localization to nerve terminals. Proc. Natl. Acad. Sci. USA *92*, 3161–3165.

Rusakov, D.A., and Fine, A. (2003). Extracellular Ca2+ depletion contributes to fast activity-dependent modulation of synaptic transmission in the brain. Neuron *37*, 287–297.

Ryan, T.A., Smith, S.J., and Reuter, H. (1996). The timing of synaptic vesicle endocytosis. Proc. Natl. Acad. Sci. USA *93*, 5567–5571.

Sakmann, B., and Neher, E. (1995). Geometric parameters of pipettes and membrane patches. In Single-Channel Recording, B. Sakmann and E. Neher, eds. (New York: Plenum Press), pp. 637–650.

Schmalzing, G. (1985). Mechanism of depolarization of rat cortical synaptosomes at submicromolar external Ca2+ activity. The use of Ca2+ buffers to control the synaptosomal membrane potential. Biochem. J. *225*, 671–680.

Shibuki, K. (1990). Activation of neurohypophysial vasopressin release by Ca2+ influx and intracellular Ca2+ accumulation in the rat. J. Physiol. *422*, 321–331.

Smith, S.J. (1992). Do astrocytes process neural information? Prog. Brain Res. *94*, 119–136.

Southan, A.P., and Robertson, B. (1998). Patch-clamp recordings from cerebellar basket cell bodies and their presynaptic terminals reveal an asymmetric distribution of voltage-gated potassium channels. J. Neurosci. *18*, 948–955.

Stanley, E.F. (2000). Presynaptic calcium channels and the depletion of synaptic cleft calcium ions. J. Neurophysiol. *83*, 477–482.

Sun, X.P., Schlichter, L.C., and Stanley, E.F. (1999). Single-channel properties of BK-type calcium-activated potassium channels at a cholinergic presynaptic nerve terminal. J. Physiol. *518*, 639–651.

Vassilev, P.M., Mitchel, J., Vassilev, M., Kanazirska, M., and Brown, E.M. (1997). Assessment of frequency-dependent alterations in the level of extracellular Ca2+ in the synaptic cleft. Biophys. J. *72*, 2103–2116.

Xiong, Z., Lu, W., and MacDonald, J.F. (1997). Extracellular calcium sensed by a novel cation channel in hippocampal neurons. Proc. Natl. Acad. Sci. USA *94*, 7012–7017.

Ye, C., Ho-Pao, C.L., Kanazirska, M., Quinn, S., Seidman, C.E., Seidman, J.G., Brown, E.M., and Vassilev, P.M. (1997). Deficient cation channel regulation in neurons from mice with targeted disruption of the extracellular Ca2+-sensing receptor gene. Brain Res. Bull. *44*, 75–84.

Zhang, E.T., Hansen, A.J., Wieloch, T., and Lauritzen, M. (1990). Influence of MK-801 on brain extracellular calcium and potassium activities in severe hypoglycemia. J. Cereb. Blood Flow Metab. *10*, 136–139.